Multiples: signal or noise?

Journal:	*Geophysics*
Manuscript ID:	GEO-2014-0486
Manuscript Type:	Technical Paper
Date Submitted by the Author:	12-Nov-2014
Complete List of Authors:	Weglein, Arthur; University of Houston, Physics;
Keywords:	multiples, noise, processing, imaging
Area of Expertise:	Tutorials and Expository Discussions, Seismic Migration
Note: The following files were submitted by the author for peer review, but cannot be converted to PDF. You must view these files (e.g. movies) online.	
Figures.zip	

Multiples: signal or noise?

Arthur B. Weglein

M-OSRP/Physics Dept./University of Houston

November 12, 2014

Abstract

There has been considerable recent interest and activity (for example, published papers, international conference presentations and workshops) on the topic of using multiples as signal. Those pursuing this use of multiples as signal state that they seek to enhance the imaging of primaries by imaging both primaries and multiples. In this paper, we unambiguously show, for the first time, that by following every individual surface recorded event (primary, free surface multiple and internal multiple events) in the most definitive, quantitative and solid physics based migration process, originally pioneered and provided by Jon Claerbout, and an accurate discontinuous velocity and density model, that only the recorded primaries enter migration and migration-inversion. We explain and help clarify that those who claim to "migrate multiples" are, in fact, not migrating multiples, but are actually using a recorded multiple and a recorded primary subevent of the multiple, to predict an unrecorded primary subevent of that multiple. The multiple is being used to predict an unrecorded primary. The recorded primaries and the unrecorded primaries, that are (ap-

proximately) predicted, can form a more complete set of primaries for migration. Once an enhanced set of primaries is achieved, we have a data set consisting of recorded and predicted primaries, and free surface and internal multiples. In practice, we employ smooth velocity models, and free surface and internal multiples will produce false images. That reality has been, and remains, the reason that multiples need to be removed before imaging. An event is useful if it can assist with providing unrecorded primaries, and multiples can be classified as useful. However, if signal relates to events that actually contribute to how we locate and delineate targets, then primaries are signal and multiples are noise. Before migration and migration-inversion, multiples need to be effectively removed without damaging primaries.

Introduction

To begin, "signal" within the context of exploration seismology, and for the purpose of this paper, refers to the **events** in seismic recorded data used for extracting subsurface information. Migration and migration-inversion are the methods used to determine subsurface information from recorded seismic data. Methods that employ the wave equation for migration have two ingredients: (1) a wave propagation concept and (2) an imaging condition. Claerbout (1971) pioneered and developed three imaging conditions for seismic migration. He combined these imaging conditions with one-way wave propagation concepts to determine structure at depth. Claerbout's three landmark imaging conditions are: (1) the exploding reflector model, (2) the space and time coincidence of up and down waves, and (3) the pre-

dicted coincident source and receiver experiment at depth, at time equals zero. The third imaging condition stands alone for clarity and definitiveness and in its potential to be extended for detailed angle dependent amplitude analysis at the target. The third imaging condition predicts an actual seismic experiment at depth, and that predicted experiment consists of all the events that experiment would record, if you had a source and receiver at that subsurface location. That experiment would have its own recorded events, the primaries and multiples for that predicted experiment. Stolt and his colleagues (Clayton and Stolt, 1981; Stolt and Weglein, 1985; Stolt and Benson, 1986; Weglein and Stolt, 1999; Stolt and Weglein, 2012) then provided the extension, for one way waves, of the Claerbout source and receiver experiment imaging condition (Imaging condition III) to allow for non coincident source and receiver at time equals zero, to realize both structural and inversion objectives. Due to causality, the offset dependence, at time equals zero, is highly localized about zero offset. The character of that singular function, sharply peaked in offset, is smooth in offset wave-number, where the extraction of angle dependent reflection information naturally occurs. The latter extension and generalization produced migration-inversion (Stolt and Weglein, 1985), or first determining where anything changed (migration) followed by what specifically changed (inversion) at the image location. Recently, several papers by Weglein and his colleagues (Weglein et al., 2011a,b; Liu and Weglein, 2014) provided the next step in the evolution of migration based on the Claerbout predicted source and receiver experiment imaging condition (Imaging condition III), extending the prediction of the source and receiver experiment in a volume within which there are two way propa-

gating waves. The latter method of imaging based on Imaging condition III for a medium with two way propagating waves, plays a central role in the analysis of this paper. The predicted experiment, in the volume is realized by calling upon Green's theorem and a Green's function that along with its normal derivative vanishes on the lower portion of the closed surface.

All current RTM methods, for two way waves, are extensions and/or variants of the second of Claerbout's imaging conditions, and do not correspond to Claerbout's imaging condition III a source and receiver experiment at depth.

Migration of two-way propagating waves

One doesn't have to look very far to find an example of the need for a predicted experiment at depth at points in a volume where there is two way wave propagation. Imaging from above or below a single horizontal reflector requires that two way wave propagation and Claerbout's predicted experiment imaging condition. Predicting a source and receiver experiment to locate and to determine the reflection coefficient from above, and, separately, from below, a single reflector requires predicting a source and receiver experiment inside a volume with two way propagating waves two way wave migration, since the reflection data is upgoing (to a source and receiver experiment located) above the reflector and is downgoing (to that experiment when the source and receiver are located) below the reflector. Of course, the addition of, for example, multiples and/or diving waves also represent examples of two way wave propagation in the region where you want to

predict the seismic experiment at depth.

As we mentioned, migration methods that employ the wave equation have two ingredients: (1) a wave propagation or prediction model and (2) an imaging condition.

For the purposes of this discussion we are going to adopt the Claerbout predicted coincident source and receiver experiment at time equals zero imaging condition for its peerless clarity, generality and quantitative information value. In the next section, we describe the evolution of the prediction of the source and receiver experiment component of Claerbout imaging condition III.

To predict the source and receiver experiment at depth

The elastic and firm mathematical physics foundation for predicting a wavefield inside a volume from (measured) values on the surface bounding the volume was provided by Green (1828) as variants of what we now call Green's theorem. In the next several sections, we describe the evolution and application of Green's theorem for predicting the source and receiver experiment at depth, since that is an essential step in tracing the realization and application of Claerbout's imaging condition III. In that evolution, we will begin with: (1) the original infinite hemisphere volume model, then (2) the reasoning, need for, and description of finite volume model for one way waves, and finally, (3) the need for and description of the finite volume model prediction of the source and receiver experiment for two way waves.

The material presented below on the evolution of the predicted source and receiver experiment has been published previously in the cited references. We cite and follow those references, but include that in this paper, for: (1) ease of the references, and (2) to make this paper self contained, and (3) because it plays such a critical role in Claerbout imaging III, which in turn is essential to understand the new message that this paper is communicating.

The infinite hemispherical migration model

The earliest wave equation migration pioneers considered the subsurface volume where the source and receiver experiment would be predicted as an infinite hemispherical half space with known mechanical properties, whose upper plane surface corresponded to the measurement surface, as in, *e.g.*, Schneider (1978) and Stolt (1978). See Figure 1.

Those two papers each made a tremendous conceptual and practical contribution to seismic imaging and exploration seismology. However, there are several problems with the infinite hemispherical migration model. That model assumes: (1) that all subsurface properties beneath the measurement surface (MS) are known, and (2) that an anticausal Green's function (*e.g.*, Schneider (1978)), with a Dirichlet boundary condition on the measurement surface, would allow measurements (MS) of the wavefield, P, on the upper plane surface of the hemisphere to determine the value of P within the hemispherical volume, V. The first assumption leads to the contradiction that we have not allowed for anything that is unknown to be determined

in our model, since everything within the closed and infinite hemisphere is assumed to be known. Within the infinite hemispherical model there is nothing and/or nowhere below the measurement surface where an unknown scattering point or reflection surface can serve to produce reflection data whose generating reflectors are initially unknown and being sought by the migration process.

The second assumption, in early infinite hemispherical wave equation migration, assumes that Green's theorem with wavefield measurements on the upper plane surface and using an anticausal Green's function satisfying a Dirichlet boundary condition can determine the wavefield within V. That conclusion assumes that the contribution from the lower hemispherical surface of S vanishes as the radius of the hemisphere goes to infinity. That is not the case, as we explicitly demonstrate below. To examine the various large radius hemispherical surface contributions to Green's theorem wave prediction in a volume, it is instructive to review the relationship between Green's theorem and the Lippmann-Schwinger scattering equation.

Green's theorem review (the Lippmann-Schwinger Equation and Green's theorem)

We begin with a space and time domain Green's theorem. Consider two wavefields P and G_0 that satisfy

$$(\nabla^2 - \frac{1}{c^2}\partial_t^2)P(\mathbf{r},t) \quad = \quad \rho(\mathbf{r},t) \tag{1}$$

and

$$(\nabla^2 - \frac{1}{c^2}\partial_t^2)G_0(\mathbf{r}, t, \mathbf{r}', t') \quad = \quad \delta(\mathbf{r} - \mathbf{r}')\delta(t - t'), \tag{2}$$

where we assume 3D wave propagation and the wavefield velocity c is a constant. ρ is a general source, *i.e.*, it represents both active sources (air guns, dynamite, vibrator trucks) and passive sources (heterogeneities in the earth). The causal solution to equation 1 can be written as

$$P(\mathbf{r}, t) = \int_{-\infty}^{t^+} dt' \int_{\infty} d\mathbf{r}' \rho(\mathbf{r}', t') G_0^+(\mathbf{r}, t, \mathbf{r}', t'), \tag{3}$$

where G_0^+ is the causal whole space solution to equation 2 and $t^+ = t + \epsilon$ where ϵ is a small positive quantity. The integral from t^+ to ∞ is zero due to the causality of G_0^+ (please see Morse and Feshbach, 1981, page 836). Equation 3 represents the linear superposition of causal solutions G_0^+ with weights $\rho(\mathbf{r}', t')$ summing to produce the physical causal wavefield solution to equation 1. Equation 3 is called the scattering equation and represents an all space and all time causal solution for $P(\mathbf{r}, t)$. It explicitly includes all sources and produces the field at all points of space and time. No additional boundary or initial conditions are required in equation 3.

Now consider the integral

$$\begin{aligned} &\int_0^{t^+} dt' \int_V d\mathbf{r}' (P\nabla'^2 G_0 - G_0 \nabla'^2 P) \\ &= \int_0^{t^+} dt' \int_V d\mathbf{r}' \nabla' \cdot (P\nabla' G_0 - G_0 \nabla' P), \end{aligned} \tag{4}$$

and we rewrite equation 4 using Green's theorem

$$\int_0^{t^+} dt' \int_V d\mathbf{r}' \nabla' \cdot (P\nabla' G_0 - G_0 \nabla' P)$$
$$= \int_0^{t^+} dt' \int_S dS' \hat{n} \cdot (P\nabla' G_0 - G_0 \nabla' P). \quad (5)$$

This is essentially an identity, within the assumptions on functions and surfaces, needed to derive Green's theorem. Now choose $P = P(\mathbf{r}', t')$ and $G_0 = G_0(\mathbf{r}, t, \mathbf{r}', t')$ from equations 1 and 2. Then replace $\nabla'^2 P$ and $\nabla'^2 G_0$ from the differential equations 1 and 2.

$$\nabla'^2 G_0 = \frac{1}{c^2}\partial_t'^2 G_0 + \delta(\mathbf{r} - \mathbf{r}')\delta(t - t') \quad (6)$$
$$\nabla'^2 P = \frac{1}{c^2}\partial_t'^2 P + \rho(\mathbf{r}', t'), \quad (7)$$

and assume that the out variables $(\mathbf{r}, t)$ are in the intervals of integration: $\mathbf{r}$ in V, $t > 0$. The left hand side of equation 4 becomes:

$$\int_0^{t^+} dt' \int_V d\mathbf{r}' \frac{1}{c^2}(P\partial_{t'}^2 G_0 - G_0 \partial_{t'}^2 P) + P(\mathbf{r}, t)$$
$$- \int_0^{t^+} dt' \int_V d\mathbf{r}' \rho(\mathbf{r}', t') G_0(\mathbf{r}, t, \mathbf{r}', t'). \quad (8)$$

The expression inside the first set of parentheses is a perfect derivative

$\partial_{t'}(P\partial_{t'}G_0 - G_0\partial_{t'}P)$ integrated over t'. The result is (for $\mathbf{r}$ in V and $t > 0$)

$$\begin{aligned} P(\mathbf{r},t) = &\int_V d\mathbf{r}' \int_0^{t^+} dt' \rho(\mathbf{r}',t') G_0(\mathbf{r},t,\mathbf{r}',t') \\ &- \frac{1}{c^2}\Big|_{t'=0}^{t^+} \int_V d\mathbf{r}' [P\partial_{t'}G_0 - G_0\partial_{t'}P] \\ &+ \int_0^{t^+} dt' \int_S dS' \hat{n} \cdot (P\nabla' G_0 - G_0 \nabla' P). \end{aligned} \tag{9}$$

We assumed differential equations 6 and 7 in deriving equation 9 and G_0 can be any solution of equation 6 in the space and time integrals in equation 4, causal, anticausal, or neither. Each term on the right hand side of equation 9 will differ with different choices of G_0, but the sum of the three terms will always be the same, $P(\mathbf{r},t)$.

If we now choose G_0 to be causal ($= G_0^+$) in equation 9, then in the second term on the right hand side the upper limit gives zero because G_0^+ and $\partial_{t'}G_0^+$ are zero at $t' = t^+$. The causality of G_0^+ and $\partial_{t'}G_0^+$ causes only the lower limit $t' = 0$ to contribute in

$$-\frac{1}{c^2}\Big|_{t'=0}^{t^+} \int_V d\mathbf{r}' [P\partial_{t'}G_0^+ - G_0^+\partial_{t'}P]. \tag{10}$$

If we let the space and time limits in equation 9 both become unbounded, *i.e.*, $V \to \infty$ and the t' interval becomes $[-\infty, 0]$, and choose $G_0 = G_0^+$, the whole space causal Green's function, then by comparing equations 3 and 9

we see that for $\mathbf{r}$ in V and $t > 0$ that

$$\int_{-\infty}^{t^+} dt' \int_S dS' \hat{n} \cdot (P \nabla' G_0^+ - G_0^+ \nabla' P) - \frac{1}{c^2} \Big|_{-\infty}^{t^+} \int_\infty d\mathbf{r}' [P \partial_{t'} G_0^+ - G_0^+ \partial_{t'} P] = 0. \quad (11)$$

$V = \infty$ means a volume that spans all space, and $\infty - V$ means all points in ∞ that are outside the volume V. For $\mathbf{r}$ in ∞ and any time t from equation 3 we get

$$\begin{aligned} P(\mathbf{r},t) = &\int_V d\mathbf{r}' \int_0^{t^+} dt' \rho(\mathbf{r}',t') G_0^+(\mathbf{r},t,\mathbf{r}',t') \\ &+ \int_{\infty - V} d\mathbf{r}' \int_0^{t^+} dt' \rho(\mathbf{r}',t') G_0^+(\mathbf{r},t,\mathbf{r}',t') \\ &+ \int_V d\mathbf{r}' \int_{-\infty}^0 dt' \rho(\mathbf{r}',t') G_0^+(\mathbf{r},t,\mathbf{r}',t') \\ &+ \int_{\infty - V} d\mathbf{r}' \int_{-\infty}^0 dt' \rho(\mathbf{r}',t') G_0^+(\mathbf{r},t,\mathbf{r}',t'). \end{aligned} \quad (12)$$

This equation holds for any $\mathbf{r}$ and any t.

For $\mathbf{r}$ in V and $t > 0$ equations 12 and 9 must agree and

$$\begin{aligned} &- \frac{1}{c^2} \Big|_0^{t^+} \int_V d\mathbf{r}' [P \partial_{t'} G_0^+ - G_0^+ \partial_{t'} P] \\ &= \int_V d\mathbf{r}' \int_{-\infty}^0 dt' \rho(\mathbf{r}',t') G_0^+(\mathbf{r},t,\mathbf{r}',t') \\ &+ \int_{\infty - V} d\mathbf{r}' \int_{-\infty}^0 dt' \rho(\mathbf{r}',t') G_0^+(\mathbf{r},t,\mathbf{r}',t') \end{aligned} \quad (13)$$

and

$$\int_0^{t^+} dt' \int_S dS' \hat{n} \cdot [P\nabla' G_0 - G_0 \nabla' P]$$
$$= \int_{\infty - V} d\mathbf{r}' \int_0^{t^+} dt' \rho(\mathbf{r}', t') G_0^+(\mathbf{r}, t, \mathbf{r}', t'). \quad (14)$$

The solution for $P(\mathbf{r}, t)$ in equation 3 expresses the fact that if all of the factors that both create the wavefield (active sources) and that subsequently influence the wavefield (passive sources, *e.g.*, heterogeneities in the medium) are explicitly included in the solution as in equation 9, then the causal solution is provided explicitly and linearly in terms of those sources, as a weighted sum of causal solutions, and no surface, boundary or initial conditions are necessary or required.

From equations 13 and 14 the role of boundary and initial conditions are clear. The contributions to the wavefield, P, at a point $\mathbf{r}$ in V and at a time, t in $[0, t^+]$ derives from three contributions: (1) a causal superposition over the sources within the volume V during the interval of time, say $[0, t^+]$ and (2) initial conditions of P and P_t over the volume V, providing all contributions due to sources earlier than time $t' = 0$, both inside and outside V, to the solution in V during $[0, t]$ and (3) a surface integral, enclosing V, integrated from $t' = 0$ to t^+ that gives the contribution from sources outside V during the time $[0, t^+]$ to the field, P, in V for times $[0, t^+]$. Succinctly stated, initial conditions provide contributions from sources at earlier times and surface/boundary conditions provide contributions from outside the spatial volume to the field in the volume during the $[0, t]$ time interval. If all sources for all space and all time are explicitly included as in equation 3, then there

is no need for boundary or initial conditions to produce the physical/causal solution derived from a linear superposition of elementary causal solutions.

On the other hand, if we seek to find a physical causal solution for P in terms of a linear superposition of anticausal solutions, as we can arrange by choosing $G_0 = G_0^-$ in equation 9, then the initial and surface integrals do not vanish when we let $V \to \infty$ and $[0, t] \to [-\infty, t]$. The vanishing of the surface integral contribution (as the radius of the surface $\to \infty$) to P with the choice $G_0 = G_0^+$ is called the Sommerfeld radiation condition, and is readily understood by the comparison with equation 3.

In the $(\mathbf{r}, \omega)$ domain equations 1 and 2 become

$$(\nabla^2 + k^2)P(\mathbf{r}, \omega) = \rho(\mathbf{r}, \omega) \tag{15}$$

$$(\nabla^2 + k^2)G_0(\mathbf{r}, \mathbf{r}', \omega) = \delta(\mathbf{r} - \mathbf{r}'), \tag{16}$$

and the causal all space and time solution analogous to equation 3 is

$$P(\mathbf{r}, \omega) = \int_\infty d\mathbf{r}' \rho(\mathbf{r}', \omega) G_0^+(\mathbf{r}, \mathbf{r}', \omega), \tag{17}$$

and Green's second identity is

$$\int_V d\mathbf{r}' (P\nabla'^2 G_0 - G_0 \nabla'^2 P) = \oint_S dS'\, \hat{n} \cdot (P\nabla' G_0 - G_0 \nabla' P). \tag{18}$$

Substituting $\nabla^2 G_0 = -k^2 G_0 + \delta$ and $\nabla^2 P = -k^2 P + \rho$ in Green's theorem

where $\int_{-\infty}^{\infty} P(\mathbf{r},t)e^{i\omega t}dt = P(\mathbf{r},\omega)$ we find

$$\int_V d\mathbf{r}' P(\mathbf{r}',\omega)\delta(\mathbf{r}-\mathbf{r}') = \int_V d\mathbf{r}' \rho(\mathbf{r}',\omega)G_0(\mathbf{r},\mathbf{r}',\omega) + \oint_S dS'\hat{n}\cdot(P\nabla' G_0 - G_0\nabla' P), \qquad (19)$$

if $\mathbf{r}$ in V. There are no initial conditions, since in $\mathbf{r},\omega$ we have already explicitly included all time in Fourier transforming from t to ω. All times of sources are included in the $(\mathbf{r},\omega)$ domain. In $\mathbf{r},\omega$ the only issue is whether sources are inside or outside V. The Lippmann-Schwinger equation (17) provides the causal physical P for all $\mathbf{r}$. Equation 17 is the $\mathbf{r},\omega$ version of equation 3 and must choose $G_0 = G_0^+$ (causal) to have P as the physical solution built from superposition and linearity. In contrast, equation 19 (as in equation 9) will produce the physical solution, P, with any solution for G_0 that satisfies equation 16.

Equation 17 can be written as:

$$\int_V \rho G_0^+ + \int_{\infty - V} \rho G_0^+. \qquad (20)$$

For $\mathbf{r}$ in V the second term on the right hand side of equation 19 (with $G_0 = G_0^+$) equals the second term in equation 20, *i.e.*,

$$\int_{\infty - V} d\mathbf{r}' \rho G_0^+ = \oint_S dS'\hat{n}\cdot(P\nabla' G_0^+ - G_0^+\nabla' P). \qquad (21)$$

Thus, the first term in equation 20 gives contribution to P, for $\mathbf{r}$ in V due to sources in V, and the second term in equation 20 gives contribution to

P, for $\mathbf{r}$ in V due to sources not in V. With $G_0 = G_0^+$

$$\oint_S dS' \hat{n} \cdot (P \nabla' G_0^+ - G_0^+ \nabla' P), \tag{22}$$

provides the contribution to the field, P, inside V due to sources outside the volume V.

What about the large $|\mathbf{r}|$ contribution of the surface integral to the field inside the volume? We use Green's theorem to predict that the contribution to the physical/causal solution P in V from the surface integral in Green's theorem, in general, and also

$$\oint_S \{P \frac{\partial G_0^+}{\partial n} - G_0^+ \frac{\partial P}{\partial n}\} dS, \tag{23}$$

vanishes as $|\mathbf{r}| \to \infty$ and in contrast the contribution to P in V from

$$\oint_S \{P \frac{\partial G_0^-}{\partial n} - G_0^- \frac{\partial P}{\partial n}\} dS, \tag{24}$$

does not vanish as $|\mathbf{r}| \to \infty$.

We begin with equation 19

$$\underset{\mathbf{r} \text{ in V}}{P(\mathbf{r}, \omega)} = \int_V d\mathbf{r}' \rho(\mathbf{r}', \omega) G_0^{\pm}(\mathbf{r}, \mathbf{r}', \omega) + \oint_S dS' \{P \frac{\partial G_0^{\pm}}{\partial n} - G_0^{\pm} \frac{\partial P}{\partial n}\} \tag{25}$$

with G_0 either causal G_0^+ or anticausal G_0^-. When $|\mathbf{r}| \to \infty$, the contribution from the second term on the right hand side of equation 25 to P in V must

go to 0, following a comparison with

$$P(\mathbf{r},\omega) = \int_{\infty} d\mathbf{r}'\rho(\mathbf{r}',\omega)G_0^+(\mathbf{r},\mathbf{r}',\omega), \tag{26}$$

(the Lippmann-Schwinger equation). However, as $|\mathbf{r}| \to \infty$, with $G_0 = G_0^-$,

$$\begin{aligned} &\oint_{S\to\infty} dS'\{P\frac{\partial G_0^-}{\partial n} - G_0^-\frac{\partial P}{\partial n}\} + \int_{V\to\infty} d\mathbf{r}'\rho(\mathbf{r}',\omega)G_0^-(\mathbf{r},\mathbf{r}',\omega) \\ &= \int_{V\to\infty} d\mathbf{r}'\rho(\mathbf{r}',\omega)G_0^+(\mathbf{r},\mathbf{r}',\omega) + 0, \end{aligned} \tag{27}$$

so

$$\begin{aligned} &\oint_{S\to\infty} \{P\frac{\partial G_0^-}{\partial n} - G_0^-\frac{\partial P}{\partial n}\}dS \\ &= \int_{\infty} [G_0^+(\mathbf{r},\mathbf{r}',\omega) - G_0^-(\mathbf{r},\mathbf{r}',\omega)]\rho(\mathbf{r}',\omega)d\mathbf{r}' \neq 0 \end{aligned} \tag{28}$$

for all time. Hence, the large distance surface contribution to the physical field, P, within V with the surface values of the physical field P and $\partial P/\partial n$ and an anticausal Green's function G_0^- will not vanish as $|\mathbf{r}| \to \infty$. As we mentioned earlier, this is one of the two problems with the infinite hemisphere model of seismic migration.

Although

$$P(\mathbf{r},\omega) = \int_{\infty} d\mathbf{r}'\rho(\mathbf{r}',\omega)G_0^-(\mathbf{r},\mathbf{r}',\omega), \tag{29}$$

would be a solution to equations 1 and 15 for all $\mathbf{r}$, it would not be the causal/physical solution to equations 1 and 15. And hence, in summary the

contribution to the causal/physical solution for $P(\mathbf{r},\omega)$ for $\mathbf{r}$ in V from

$$\int_S dS' \left(P \frac{dG_0^+}{dn} - G_0^+ \frac{dP}{dn} \right), \tag{30}$$

goes to zero as $|R| \rightarrow \infty$ where P and dP/dn corresponds to physical/causal boundary values of P and dP/dn, respectively. Physical measurements of P and dP/dn on S are always causal/physical values. The integral

$$\int_S dS' \left(P \frac{dG_0^-}{dn} - G_0^- \frac{dP}{dn} \right), \tag{31}$$

does not go to zero for anti-causal, G_0^-, and causal/physical P and dP/dn. The latter fact bumps up against a key assumption in the infinite hemisphere models of migration. That combined with the fact the infinite hemisphere model assumes the entire subsurface, down to "infinite" depth is known, suggests the need for a different model. That model is the finite volume model (see, *e.g.*, Weglein et al., 2011a,b).

Finite volume model for migration

The finite model for migration assumes that we know or can adequately estimate earth medium properties (*e.g.*, velocity) down to the reflector we seek to image. The finite volume model assumes that beneath the sought after reflector the medium properties are, and will remain, unknown. The "finite volume model" corresponds to the volume within which we assume the earth properties are known and within which we predict the wavefield from surface measurements. We have moved away from the two issues of the

infinite hemisphere model, *i.e.*, (1) the assumption we know the subsurface to all depths and (2) that the surface integral with an anticausal Green's function has no contribution to the field being predicted in the earth.

The finite volume model removes both of the problematic assumptions behind the infinite hemisphere model. However, we are now dealing with a finite volume V, and with a surface S, consisting of upper surface S_U, lower surface S_L and walls, S_W (Figure 2). We only have measurements on S_U. In the following sections on: (1) Green's theorem for one-way propagation; and (2) Green's theorem for two-way propagation we show how the choice of Green's function allows the finite volume migration model to be realized. The construction of the Green's function that can accommodate two-way propagation in V, from contributions only on S_U, is a new contribution (Weglein et al., 2011a,b) that allows Claerbout Imaging III to be realized in a volume with two-way propagating waves. That places RTM on a firm wave theoretical Green's theorem basis, for the first time, with algorithmic consequence and with a clear consistent understanding of the amplitude of the RTM image. The new Green's function is neither causal, anticausal, nor a combination of causal and/or anticausal Green's functions. In the important paper by Amundsen (1994), a finite volume model for wavefield prediction is developed which requires knowing (*i.e.*, predicting through solving an integral equation) for the wavefield at the lower surface. In parts I and II we show that for one and two-way propagation, respectively, that with a proper and distinct choice of Green's function, in each case, that absolutely no wavefield measurement information on the lower surface is required or needs to be estimated/predicted. Below, we review how to choose

the Green's functions that allow for two-way propagation (for RTM application) without the need for measurements on the lower boundary of the closed surface in Green's theorem.

Finite volume model for migration (Claerbout Imaging Condition III): Green's theorem for predicting the source and receiver experiment for one way waves

Consider a 1D upgoing plane wavefield $P = Re^{-ikz}$ propagating upward through the 1D homogeneous volume without sources between $z = a$ and $z = b$ (Figure 3). The wave P inside V can be predicted from

$$P(z,\omega) \;=\; \Big|_{z'=a}^{b} \{P(z',\omega)\; \frac{dG_0}{dz'}(z,z',\omega) - G_0(z,z',\omega)\frac{dP}{dz'}(z',\omega)\} \qquad (32)$$

with a Green's function, G_0, that satisfies

$$\left(\frac{d^2}{dz'^{\,2}} + k^2\right)\; G_0(z,z',\omega) \;=\; \delta(z-z') \qquad (33)$$

for z and z' in V. We can easily show that for an upgoing wave, $P = Re^{-ikz}$, that if one chooses $G_0 \;=\; G_0^+$ (causal, $e^{ik|z-z'|}/(2ik)$), the lower surface (i.e. $z' \;=\; b$) constructs P in V and the contribution from the upper surface vanishes. On the other hand, if we choose $G_0 = G_0^-$ (anticausal solution $e^{-ik|z-z'|}/(-2ik)$), then the upper surface $z = a$ constructs $P = Re^{-ikz}$ in V and there is no contribution from the lower surface $z' = b$. This makes

sense since information on the lower surface $z' = b$ will move with the upwave into the region between a and b, with a forward propagating causal Green's function, G_0^+. At the upper surface $z' = a$, the anticausal G_0^- will predict from an upgoing wave measured at $z' = a$, where the wave was previously and when it was moving up and deeper than $z' = a$.

Since in exploration seismology the reflection data is typically upgoing, once it is generated at the reflector, and we only have measurements at the upper surface $z' = a$, we choose an anticausal Green's function G_0^- in one-way wave prediction in the finite volume model. If in addition we want to rid ourselves of the need for dP/dz' at $z' = a$ we can impose a Dirichlet boundary condition on G_0^-, to vanish at $z' = a$. The latter Green's function is labeled G_0^{-D},

$$G_0^{-D} \;=\; -\frac{e^{-ik|z-z'|}}{2ik} - \left(-\frac{e^{-ik|z_I-z'|}}{2ik}\right), \tag{34}$$

where z_I is the image of z through $z' = a$. It is easy to see that $z_I = 2a - z$ and that

$$P(z) \;=\; -\frac{dG_0^{-D}}{dz'}(z,z',\omega)\Big|_{z'=a} P(a) \;=\; e^{-ik(z-a)}P(a), \tag{35}$$

in agreement with a simple Stolt FK phase shift for predicting an upward propagating wave in a volume. Please note that $P(z,\omega) = -dG_0^{-D}/dz'(z,z',\omega)|_{z'=a}P(a,\omega)$ back propagates $P(z' = a,\omega)$, not G_0^{-D}. The latter thinking that G_0^{-D} back propagates data is a fundamental mistake/flaw in many seismic back propagation migration and inversion theories, that (as

is clear from this example) leads to amplitude issues and errors.

The multidimensional 3D generalization for predicting an experiment at depth with both sources and receivers for an upgoing wavefield in the volume is as follows:

$$\begin{aligned} & \int \frac{dG_0^{-D}}{dz_s}(x'_s, y'_s, z'_s, x_s, y_s, z_s; \omega) \\ & \times \left[\int \frac{dG_0^{-D}}{dz_g}(x'_g, y'_g, z'_g, x_g, y_g, z_g; \omega) D(x'_g, y'_g, z'_g, x'_s, y'_s, z'_s; \omega) dx'_g dy'_g \right] dx'_s dy'_s \\ = \; & M(x_s, y_s, z_s, x_g, y_g, z_g; \omega) \\ = \; & M(x_m, y_m, z_m, x_h, y_h, z_h; \omega), \end{aligned} \tag{36}$$

where $x_g + x_s = x_m$, $y_g + y_s = y_m$, $z_g + z_s = z_m$, $x_g - x_s = x_h$, $y_g - y_s = y_h$, and $z_g - z_s = z_h$. The uncollapsed migration is $M(x_m, y_m, z_m, x_h, y_h, z_h = 0; t = 0)$ has extended and generalized the original Imaging Condition III, to non-zero offset at time equals zero, and is ready for subsequent AVO analysis in a multi-D subsurface (see *e.g.* Clayton and Stolt (1981), Stolt and Weglein (1985), Weglein and Stolt (1999)).

The Green's function for two-way propagation that will eliminate the need for data at the lower surface of the closed Green's theorem surface is found by finding a general solution to the Green's function for the medium in the finite volume model and imposing both Dirichlet and Neumann boundary conditions at the lower surface.

Predicting the source and receiver experiment at depth in a finite volume where the velocity configuration is $c(x, y, z)$

Step (1) For a receiver predicted at a point (x, y, z) for determining $P(x, y, z, x_s, y_s, z_s, \omega)$, call on the Green's function, G_0, that satisfies

$$\left\{\nabla'^2 + \frac{\omega^2}{c^2(x', y', z')}\right\} G_0(x', y', z', x, y, z, \omega)$$
$$= \delta(x - x')\delta(y - y')\delta(z - z') \tag{37}$$

for a source at (x, y, z). P is the physical/causal solution satisfying

$$\left\{\nabla'^2 + \frac{\omega^2}{c^2(x', y', z')}\right\} P(x', y', z', x_s, y_s, z_s, \omega)$$
$$= A(\omega)\delta(x' - x_s)\delta(y' - y_s)\delta(z' - z_s). \tag{38}$$

As a first step, we want to predict P for a point (x, y, z) in the volume V, for the actual/original source at (x_s, y_s, z_s). For (x, y, z) in V, arrange for G_0 and $\nabla' G_0 \cdot \hat{n}'$ to be zero for (x', y', z') on the lower surface S_L and the walls S_W of the finite volume. The solution for G_0 in V and on S can be found by a numerical modeling algorithm where the "source" is at (x, y, z) and the field, G_0, and $\nabla G_0 \cdot \hat{n}$ at (x', y', z') are both imposed to be zero on S_L and S_W. Once that model is run for a source at (x, y, z) for $G_0(x', y', z', x, y, z, \omega)$ [for every eventual predicted receiver point, (x, y, z), for P] where G_0 satisfies Dirichlet and Neumann conditions for (x', y', z') on S_L and S_W we output $G_0(x', y', z', x, y, z, \omega)$ for (x', y', z') on S_U (the measurement surface).

Step (2) Predict the receiver experiment at depth (with the original/actual source at (x_s, y_s, z_s))

$$\begin{aligned} & P(x, y, z, x_s, y_s, z_s, \omega) \\ = & \int \left\{ \frac{\partial G_0^{DN}}{\partial z'}(x, y, z, x', y', z', \omega) P(x', y', z', x_s, y_s, z_s, \omega) \right. \\ & \left. - \frac{\partial P}{\partial z'}(x', y', z', x_s, y_s, z_s, \omega) G_0^{DN}(x, y, z, x', y', z', \omega) \right\} dx' dy', \end{aligned} \tag{39}$$

where z' = fixed depth of the cable and (x_s, y_s, z_s) = fixed location of the source. This predicts the receiver at (x, y, z), a point below the measurement surface in the volume V.

Step (3) Now predict the experiment corresponding to the receiver and the source at depth

$$\begin{aligned} & P(x_g, y_g, z, x, y, z, \omega) \\ = & \int \left\{ \frac{\partial G_0^{DN}}{\partial z_s}(x, y, z, x_s, y_s, z_s, \omega) P(x_g, y_g, z, x_s, y_s, z_s, \omega) \right. \\ & \left. - \frac{\partial P}{\partial z_s}(x_g, y_g, z, x_s, y_s, z_s, \omega) G_0^{DN}(x, y, z, x_s, y_s, z_s, \omega) \right\} dx_s dy_s. \end{aligned} \tag{40}$$

$P(x_g, y_g, z, x, y, z, \omega)$ is the field corresponding to a predicted receiver at (x_g, y_g, z) and the source to (x, y, z) and change to midpoint offset $P(x_m, x_h, y_m, y_h, z_m, z_h = 0, \omega)$ and

$$\begin{aligned} & \int d\omega \left\{ \frac{\partial G_0^{DN}}{\partial z_s}(x, y, z, x_s, y_s, z_s, \omega) P(x_g, y_g, z, x_s, y_s, z_s, \omega) \right. \\ & \left. - \frac{\partial P}{\partial z_s}(x_g, y_g, z, x_s, y_s, z_s, \omega) G_0^{DN}(x, y, z, x_s, y_s, z_s, \omega) \right\}, \end{aligned} \tag{41}$$

and Fourier transform over x_m, x_h, y_m, y_h to find $\widetilde{P}(k_{x_m}, k_{x_h}, k_{y_m}, k_{y_h}, k_{z_m}, z_h = 0, t = 0)$. Equation 41 corresponds to Claerbout imaging condition III migration for a general $v(x, y, z)$ velocity configuration, within a volume that allows two way wave propagation.

Summary of Wave equation migration for one way and two way propagating waves

Migration and migration-inversion require velocity information for location and velocity, density, absorption... for amplitude analyses at depth. So when we say the medium is "known," the meaning of known depends on the goal: migration or migration-inversion. Backpropagation and imaging each evolved and then extended/generalized and merged into migration-inversion (Figure 4).

For one-way wave propagation the double downward continued data, D is

$$D(\text{at depth}) = \int_{S_s} \frac{\partial G_0^{-D}}{\partial z_s} \int_{S_g} \frac{\partial G_0^{-D}}{\partial z_g} D \, dS_g \, dS_s, \tag{42}$$

where D in the integrand $= D$(on measurement surface), $\partial G_0^{-D}/\partial z_s =$ anticausal Green's function with Dirichlet boundary condition on the measurement surface, $s =$ shot, and $g =$ receiver. For two-way wave double

downward continuation:

$$D(\text{at depth}) = \int_{S_s} \left[\frac{\partial G_0^{DN}}{\partial z_s} \int_{S_g} \left\{ \frac{\partial G_0^{DN}}{\partial z_g} D + \frac{\partial D}{\partial z_g} G_0^{DN} \right\} dS_g \right. \\ \left. + G_0^{DN} \frac{\partial}{\partial z_s} \int_{S_g} \left\{ \frac{\partial G_0^{DN}}{\partial z_g} D + \frac{\partial D}{\partial z_g} G_0^{DN} \right\} dS_g \right] dS_s, \quad (43)$$

where D in the integrands $= D$(on measurement surface). G_0^{DN} is *neither* causal nor anticausal. G_0^{DN} is not an *anti*causal Green's function; it is not the inverse or adjoint of any physical propagating Green's function. It is the Green's function needed for WEM RTM, that is RTM based on Claerbout Imaging Condition III. G_0^{DN} is the Green's function for the model of the finite volume that vanishes along with its normal derivative on the lower surface and the walls. If we want to use the anticausal Green's function of the two-way propagation with Dirichlet boundary conditions at the measurement surface then we can do that, but we will need measurements at depth and on the vertical walls. To have the Green's function for two-way propagation that doesn't need data at depth and on the vertical sides/walls, that requires a non-physical Green's function that vanishes along with its derivative on the lower surface and walls.

Green's theorem wavefield prediction with velocity and density variation

First, let us assume the wave propagation problem in a (one dimensional) volume V bounded by a shallower depth a and deeper depth b:

$$\left\{\frac{\partial}{\partial z'}\frac{1}{\rho(z')}\frac{\partial}{\partial z'}+\frac{\omega^2}{\rho(z')c^2(z')}\right\}D(z',\omega)=0, \tag{44}$$

where $a \leq z' \leq b$ is the depth, and $\rho(z')$ and $c(z')$ are the density and velocity fields, respectively. In exploration seismology, we let the shallower depth a be the measurement surface where the seismic acquisition takes place (please see equation 32). The volume V is the finite volume defined in the "finite volume model" for migration, the details of which can be found in Weglein et al. (2011a). We measure D at the measurement surface $z' = a$, and the objective is to predict D anywhere between the shallower surface and another surface with greater depth, $z' = b$. This can be achieved via the solution of the wave-propagation equation in the same medium by an idealized impulsive source or Green's function:

$$\left\{\frac{\partial}{\partial z'}\frac{1}{\rho(z')}\frac{\partial}{\partial z'}+\frac{\omega^2}{\rho(z')c^2(z')}\right\}G_0(z,z',\omega)=\delta(z-z'), \tag{45}$$

where z is the location of the source, and $a < z' < b$ and z increase in a downward direction. Abbreviating $G_0(z, z', \omega)$ as G_0, the solution for D in

the interval $a < z < b$ is given by Green's theorem:

$$D(z,\omega) = \frac{1}{\rho(z')}\left\{D(z',\omega)\frac{\partial G_0}{\partial z'} - G_0\frac{\partial D(z',\omega)}{\partial z'}\right\}\Bigg|_{z'=a}^{z'=b}, \tag{46}$$

where a and b are the shallower and deeper boundaries, respectively, of the volume to which the Green's theorem is applied. It is identical to equation (43) of Weglein et al. (2011a), except for the additional density contribution to the Green's theorem. Interested readers may find the derivation of equation (46) in section 2 of Liu and Weglein (2014).

Note that in equation (46), the field values on the closed surface of the volume V are necessary for predicting the field value inside V. The surface of V contains two parts: the shallower portion $z' = a$ and the deeper portion $z' = b$. In seismic exploration, the data at $z' = b$ is not available. For example, one of the significant artifacts of the current RTM procedures is caused by this phenomenon: there are events necessary for accurate wavefield prediction that reach $z' = b$ but never return to $z' = a$, as is demonstrated in Figure 5. The solution, based on Green's theorem without any approximation, was first published in Weglein et al. (2011a) and Weglein et al. (2011b), the basic idea can be summarized as follows.

Since the wave equation is a second-order differential equation, its general solution has a great deal of freedom/flexibility. In other words, for a wave equation with a specific medium property, there are an infinite number of solutions. This freedom in choosing the Green's function has been taken advantage of in many seismic-imaging procedures. For example, the most popular choice in wavefield prediction is the physical solution G_0^+. In

downward continuing a one way propagating upgoing wavefield to a point in the subsurface, the anti-causal solution G_0^- is often used in equation 46.

Weglein et al. (2011a,b) show that (with the G_0^- choice), the contribution from $z' = B$ will be zero under one way wave assumptions, and only measurements are required at $z' = A$. For two way propagating waves, G_0^- will not make the contribution for $z' = B$ vanish. However, if both G_0 and $\partial G_0/\partial z'$ vanish at the deeper boundary $z' = b$, where measurements are not available, then only the data at the shallower surface (i.e., the actual measurement surface) is needed in the calculation. We use G_0^{DN} to denote the Green's function with vanishing Dirichlet and Neumann boundary conditions at the deeper boundary.

Predicting the source and receiver at depth in a volume where the velocity and density are both variable

The original Green's theorem in equation (46) is derived to predict the wavefield (i.e., receivers) in the subsurface. It can also be used to predict the sources in the subsurface by taking advantage of reciprocity: the recording is the same after the source and receiver locations are exchanged.

Assuming we have data on the measurement surface: $D(z_g, z_s)$ (the ω dependency is ignored), we can use $G_0^{DN}(z, z_g)$ to predict it from the receiver

depth z_g to the target depth z:

$$D\left(z,z_s\right)=\frac{1}{\rho(z_g)}\left\{\frac{\partial D\left(z_g,z_s\right)}{\partial z_g}G_0^{DN}\left(z,z_g\right)-D\left(z_g,z_s\right)\frac{\partial G_0^{DN}\left(z,z_g\right)}{\partial z_g}\right\}. \tag{47}$$

Taking the $\frac{\partial}{\partial z_s}$ operation on equation (47), we have a similar procedure to predict $\partial D(z_g,z_s)/\partial z_s$ to the subsurface:

$$\frac{\partial D\left(z,z_s\right)}{\partial z_s}=\frac{1}{\rho(z_g)}\left\{\frac{\partial^2 D\left(z_g,z_s\right)}{\partial z_g\partial z_s}G_0^{DN}\left(z,z_g\right)-\frac{\partial D\left(z_g,z_s\right)}{\partial z_s}\frac{\partial G_0^{DN}\left(z,z_g\right)}{\partial z_g}\right\}. \tag{48}$$

With equations (47) and (48), we predict the data D and its partial derivative over z_s to the subsurface location z. According to reciprocity, $D\left(z,z_s\right)=E\left(z_s,z\right)$, where $E\left(z_s,z\right)$ is resulted from exchanging the source and receiver locations in the experiment to generate D at the subsurface. The predicted data $E\left(z_s,z\right)$ can be considered as the recording of receiver at z_s for a source located at z.

For this predicted experiment, the source is located at depth z, according to the Green's theorem, we can downward continue the recording at z_s to any depth shallower than or equal to z.

In seismic migration, we predict $E\left(z_s,z\right)$ at the same subsurface depth z with $G_0^{DN}\left(z,z_s\right)$ to have an experiment with coincident source and receiver:

$$\begin{aligned}E\left(z,z\right)&=\frac{1}{\rho(z_s)}\left\{\frac{\partial E\left(z_s,z\right)}{\partial z_s}G_0^{DN}\left(z,z_s\right)-E\left(z_s,z\right)\frac{\partial G_0^{DN}\left(z,z_s\right)}{\partial z_s}\right\},\\&=\frac{1}{\rho(z_s)}\left\{\frac{\partial D\left(z,z_s\right)}{\partial z_s}G_0^{DN}\left(z,z_s\right)-D\left(z,z_s\right)\frac{\partial G_0^{DN}\left(z,z_s\right)}{\partial z_s}\right\}.\end{aligned} \tag{49}$$

Depth Range	Velocity	Density
$(-\infty, a_1)$	c_0	ρ_0
(a_1, a_2)	c_1	ρ_1
(a_2, ∞)	c_2	ρ_2

Table 1: The properties of an acoustic medium with two reflectors, at depth a_1 and a_2.

If $z_s < z_g$ and we assume the data is deghosted, the $\frac{\partial}{\partial z_s}$ operation on $D(z_g, z_s)$ is equivalent to multiplying $-ik$, in this case, equation (49) can be further simplified:

$$E(z,z) = -\frac{1}{\rho(z_s)D(z,z_s)}\left\{\frac{\partial G_0^{DN}(z,z_s)}{\partial z_s} + ikG_0^{DN}(z,z_s)\right\}. \tag{50}$$

Numerical examples

As an example, for a 2-reflector model (with an ideal impulsive source located at z_s, the depth of receiver is $z_g > z_s$, the geological model is listed in Table 1), the data and its various derivatives can be expressed as:

$$\begin{aligned}
D(z_g, z_s) &= \frac{\rho_0 x^{-1}}{2ik}\left\{y + \alpha y^{-1}\right\}, \\
\frac{\partial D(z_g, z_s)}{\partial z_g} &= \frac{\rho_0}{2}x^{-1}\left\{y - \alpha y^{-1}\right\}, \\
\frac{\partial D(z_g, z_s)}{\partial z_s} &= -\frac{\rho_0}{2}x^{-1}\left\{y + \alpha y^{-1}\right\}, \\
\frac{\partial^2 D(z_g, z_s)}{\partial z_g \partial z_s} &= \frac{\rho_0 k}{2i}x^{-1}\left\{y - \alpha y^{-1}\right\},
\end{aligned} \tag{51}$$

where $x = e^{ikz_s}$, $y = e^{ikz_g}$, $\sigma = e^{ikz}$, $\alpha = e^{ik(2a_1)}\left(R_1 + (1-R_1^2)\beta\right)$, and $\beta = \sum_{n=0}^{\infty}(-1)^n R_1^n R_2^{n+1} e^{ik_1(2n+2)[a_2-a_1]}$. And $R_1 = \frac{c_1\rho_1 - c_0\rho_0}{c_1\rho_1 + c_0\rho_0}$, and $R_2 = \frac{c_2\rho_2 - c_1\rho_1}{c_2\rho_2 + c_1\rho_1}$ are the reflection coefficients from geological boundaries.

The predicted experiment above the first reflector for Claerbout Imaging Condition III

For $z < a_1$, the boundary values of the Green's function are:

$$\begin{aligned} G_0^{DN}(z, z_g) &= \rho_0 \frac{e^{ik(z-z_g)} - e^{ik(z_g-z)}}{2ik} = \rho_0 \frac{\sigma y^{-1} - \sigma^{-1} y}{2ik}, \\ G_0^{DN}(z, z_s) &= \rho_0 \frac{\sigma x^{-1} - \sigma^{-1} x}{2ik}, \\ \frac{\partial G_0^{DN}(z, z_g)}{\partial z_g} &= \rho_0 \frac{\sigma y^{-1} + \sigma^{-1} y}{-2}, \\ \frac{\partial G_0^{DN}(z, z_s)}{\partial z_s} &= \rho_0 \frac{\sigma x^{-1} + \sigma^{-1} x}{-2}. \end{aligned} \tag{52}$$

After substituting equation (51) into equation (50), we have:

$$E(z, z) = \frac{1 + e^{ik(2a_1 - 2z)}\left(R_1 + (1-R_1^2)\beta\right)}{2ik/\rho_0}. \tag{53}$$

The result above can be Fourier transformed into the time domain to have:

$$\begin{aligned} \frac{E(z, z, t)}{-\rho_0 c_0/2} =& H(t) + R_1 H(t - t_1) + (1 - R_1^2) \\ & \times \sum_{n=0}^{\infty} (-1)^n R_1^n R_2^{n+1} H(t - t_1 - (2n+2)t_2), \end{aligned} \tag{54}$$

where $t_1 = \frac{2a_1 - 2z}{c_0}$ and $t_2 = \frac{(a_2 - a_1)}{c_1}$. Balancing out the $-\frac{\rho_0 c_0}{2}$ factor*, the

*This factor is present in the incident wave, i.e., causal Green's function for a homogeneous medium with density ρ_0 and velocity c_0.

data after removing the direct wave is denoted as $\hat{D}(z,t) = \frac{-2}{\rho_0 c_0} E(z,z,t) - H(t)$:

$$\begin{aligned}\hat{D}(z,t) =& R_1 H\left(t - t_1\right) \\ &+ (1 - R_1^2) \sum_{n=0}^{\infty} (-1)^n R_1^n R_2^{n+1} H\left(t - t_1 - (2n+2)t_2\right). \end{aligned} \tag{55}$$

We take the imaging condition as first letting $z \to a_1$ through values smaller that a_1, and then (subsequently) taking the limit as $t \to 0^+$, that is, approaching zero from positive values, we find:

$$\lim_{t \to 0^+} \left(\lim_{z \to a_1^-} \hat{D}(z,t) \right) = R_1, \tag{56}$$

where

$$\begin{aligned} a_1^- &= a_1 - \epsilon_1 \qquad \epsilon_1 > 0, \\ 0^+ &= 0 + \epsilon_2 \qquad \epsilon_2 > 0, \end{aligned} \tag{57}$$

and we obtained the image of the first reflector at the actual depth a_1 with the correct reflection coefficient as amplitude.

Predicting the source and receiver experiment between the first and second reflectors

For $a_1 < z < a_2$, we have:

$$\begin{aligned} G_0^{DN}(z, z_g) &= [(R_1\lambda - \lambda^{-1})\mu + (\lambda - R_1\lambda^{-1})\mu^{-1}]/[2ik_1(1+R_1)/\rho_1], \\ \frac{\partial G_0^{DN}(z, z_g)}{\partial z_g} &= [(R_1\lambda - \lambda^{-1})\mu - (\lambda - R_1\lambda^{-1})\mu^{-1}]/[2k_1(1+R_1)/(k\rho_1)], \end{aligned} \tag{58}$$

where $\lambda = e^{ik_1(z-a_1)}$, $\mu = e^{ik(z_g-a_1)}$, $k_1 = \frac{\omega}{c_1}$. Substituting equation (58) into equation (51), and transforming the aforementioned result into the time domain, we have:

$$\begin{aligned} E(z,z,t)/(-\rho_1 c_1/2) = H(t) &+ 2\sum_{n=1}^{\infty}(-1)^n R_1^n R_2^n H\{t-[2n(a_2-a_1)/c_1]\} \\ &+ \sum_{n=0}^{\infty}(-1)^{n+1} R_1^{n+1} R_2^n H\{t-[2z+2na_2-2(n+1)a_1]/c_1\} \\ &+ \sum_{n=0}^{\infty}(-1)^n R_1^n R_2^{n+1} H\{t-[2(n+1)a_2-2na_1-2z]/c_1\}. \end{aligned} \tag{59}$$

Balancing out the $-\rho_1 c_1/2$ factor, the data after removing the direct wave is denoted as $\hat{D}(z,t) = \frac{-2}{\rho_1 c_1} E(z,z,t) - H(t)$:

$$\begin{aligned} \hat{D}(z,t) = &2\sum_{n=1}^{\infty}(-1)^n R_1^n R_2^n H\{t-[2n(a_2-a_1)/c_1]\} \\ &+ \sum_{n=0}^{\infty}(-1)^{n+1} R_1^{n+1} R_2^n H\{t-[2z+2na_2-2(n+1)a_1]/c_1\} \\ &+ \sum_{n=0}^{\infty}(-1)^n R_1^n R_2^{n+1} H\{t-[2(n+1)a_2-2na_1-2z]/c_1\}, \end{aligned} \tag{60}$$

and after taking the $t = 0^+$ imaging condition, we have:

$$\hat{D}(z,t) = \begin{cases} -R_1 & \texttt{if } (z = a_1 + \epsilon_1) \\ 0 & \texttt{if } (a_1 < z < a_2) \\ R_2 & \texttt{if } (z = a_2 - \epsilon_2) \end{cases}, \tag{61}$$

where $\epsilon_1, \epsilon_2 \to 0$ and then $t \to 0^+$. Note that in the previous section, i.e., to image above the first reflector at a_1, we obtain the amplitude R_1 when z

approach a_1 from above. In this section we image below the first reflector at a_1, the amplitude of the image is $-R_1$ when z approaches a_1 from below, as it should.

Predicting the source and receiver experiment below the second reflector

For $z > a_1$, the boundary value of the Green's function is:

$$G_0^{DN}(z, z_g) = \frac{1}{2ik_2(1+R_1)(1+R_2)/\rho_2} \tag{62}$$
$$\times \{[\nu^{-1}(R_2\lambda - \lambda^{-1}) + R_1\nu(\lambda - R_2\lambda^{-1})]\mu + [R_1\nu^{-1}(R_2\lambda - \lambda^{-1}) + \nu(\lambda - R_2\lambda^{-1})]\mu^{-1}\},$$

where $\lambda = e^{ik_2(z-a_2)}$, $\mu = e^{ik(z_g-a_1)}$, and $\nu = e^{ik_1(a_2-a_1)}$, $k_2 = \omega/c_2$.

The result of the predicted experiment can be expressed as:

$$\begin{aligned} E(z,z) =& (\rho_2/2ik_2)[1 - R_2 e^{ik_2(2z-2a_2)} + (1-R_2^2)e^{ik_2(2z-2a_2)} \\ & \times \sum_{n=0}^{\infty}(-1)^{n+1}R_1^{n+1}R_2^n e^{ik_1(2n+2)(a_2-a_1)}]. \end{aligned} \tag{63}$$

The time domain counterpart of the equation above is:

$$\begin{aligned} E(z,z,t) = -(\rho_2 c_2/2)\{&H(t) - R_2 H[t-(2z-2a_2)/c_2] \\ &+ (1-R_2^2)H[t-(2z-2a_2)/c_2 - (2n+2)(a_2-a_1)/c_1]. \end{aligned} \tag{64}$$

Balancing out the $-\rho_2 c_2/2$ factor, the data after removing the direct

wave is denoted as $\hat{D}(z,t) = (-2/\rho_2 c_2)E(z,z,t) - H(t)$:

$$\begin{aligned}\hat{D}(z,t) = &- R_2 H[t-(2z-2a_2)/c_2] \\ &+ (1-R_2^2)H[t-(2z-2a_2)/c_2 - (2n+2)(a_2-a_1)/c_1], \end{aligned} \quad (65)$$

and after taking the $t = 0^+$ imaging condition, we have:

$$\hat{D}(z,t) = \begin{cases} -R_2 & \texttt{if } (z = a_2 + \epsilon) \\ 0 & \texttt{if } (a_2 < z) \end{cases}, \quad (66)$$

where $\epsilon \to 0^+$. Note that in the previous section, i.e., to image between the first and second reflectors, we obtain the amplitude R_2 when z approach a_2 from above. In this section we image below the second reflector at a_2, the amplitude of the image is $-R_2$ when z approaches a_2 from below, as it should. Please see Figure 6.

How do the recorded events (primaries and free surface and internal multiples) contribute to: (1) the predicted source and receiver experiment at depth and (2) the image at depth that locates and identifies the reflector (the reflection coefficient)?

In this paper, we examine, follow and report (for the latter two way-wave wave migration examples) how the individual events (primaries, free surface multiples and internal multiples) each contribute to: (1) the predicted coin-

cident source and receiver experiment at each depth, and then (2) the time equals zero imaging condition evaluation of that experiment.

The example we present provides for the first time an analysis that starts with and follows how surface recorded data (with primaries and free surface and internal multiples) influences and contributes to the subsequent experiment and imaging at each depth level, and specifically: (1) how each individual recorded event in the surface data is involved and contributes to the new individual "events" of the predicted source and receiver experiment at each different depth, and then (2) what happens to the recorded surface event's individual contribution for the predicted experiment at each depth and then how the surface recorded events contribute when applying the time equals zero imaging condition. Please see three cases we examine in the three videos (http://mosrp.uh.edu/events/event-news/multiples-signal-noise-a-clear-example-with-a-definitive-conclusion) and corresponding slide snapshots. In the three examples a unit amplitude plane wave is normal incident on a one-D earth. The first case (please see Figures 7-9) is the example of a single reflector and a single primary, with no free surface or internal multiples. That single primary is the sole contributor to the events in the experiment above and below that single reflector. When the time equals zero condition is applied, the recorded primary is the only recorded event contributing to the experiment at depth and to the image, both below and above the reflector.

The second case has a single primary and a free surface multiple (please see Figures 10-12). The predicted experiment above the reflector has two surface event contributions, from the primary and the free surface multi-

ple. When the time equals zero imaging condition is applied then only the recorded primary contributes to the image. Below the reflector the predicted experiment has two events, a primary that has a downward reflection at the reflector, and a primary from the source to the free surface and then down to the predicted receiver. The original free surface multiple in the recorded data became a primary in the predicted experiment below the reflector. Hence, the primary and free surface multiple in the recorded data became two primaries for the experiment below the reflector. However, once the time equals zero imaging condition is applied to the predicted experiment, only the recorded primary contributes to the image and the recorded multiple does not.

In the third case (please see Figures 13-17), we consider a subsurface with two reflectors and two recorded primaries and one internal multiple. As you focus on the history that each individual event in the recorded data follows and then contributes to, first in the experiment at depth and then to the image at each depth, you reach the following conclusion. Recorded primaries and free surface multiples and internal multiples all contribute to events for the predicted experiment at depth. Sometimes multiples in the recorded data even become primaries in the predicted experiment at depth. However, only the recorded primaries contribute to the image at every depth. If you removed the multiples in the recorded data, the coincident source and receiver experiment at depth would change, but once the $t = 0$ imaging condition is applied not the image's location at the correct depth or its amplitude, the reflection coefficient, will not be affected. If, in these examples, your data consisted of only multiples, you would have no image

at any depth.

Hence, for the purposes of imaging and inversion, primaries are signal and multiples are not. Multiples are not evil, or bad or irresponsible, they are simply not needed for locating and identifying targets.

The methods that seek to use multiples today as "signal" are really seeking to supply primaries that have not been recorded, due to limitations in acquisition, and to address the subsequent limited illumination that missing primaries can cause. They are not really using the multiple itself as an event to be followed into the subsurface for imaging purposes. The figure (18) illustrates the idea.

Assume a multiple is recorded, and a long offset primary that is a subevent is also recorded. The idea is to extract and predict the smaller offset, and not recorded primary from the recorded multiple and the recorded longer offset primary. All the various incarnations that are using multiples as "signal" are actually, and entirely after removing a recorded longer offset primary to have the output as a shorter offset unrecorded primary. It's unrecorded primaries that the method is seeking to produce and to utilize.

The recipe of taking the multiples back in time and the primaries forward in time and arranging for Imaging Condition II (not III) produces that output.

In a Recent Advances and the Road Ahead presentation, "Multiples: signal or noise?", Weglein (2014b) (please see `https://vts.inxpo.com/scripts/Server.nxp?LASCmd=L:0&AI=1&ShowKey=21637&LoginType=0&InitialDisplay=1&ClientBrowser=0&DisplayItem=NULL&LangLocaleID=0&RandomValue=1415030021699`) showed a field data example, from PGS, where there was clear added-value

demonstrated from actual primaries, plus primaries predicted from multiples, compared to the image from the original primaries.

There is another issue: in order to predict a free surface or internal multiple, the primary sub-events that constitute the multiple must be in the data, for the multiple prediction method to recognize an event as a multiple. If the short offset primary is not recorded, the multiple that is composed of the short and long offset multiple will not be predicted as a multiple. That issue and basic contradiction within the method is recognized by those who practice this method, and instead of predicting the multiple, they use all the events in the recoded data, primaries and multiples, and the multiples can be useful for predicting missing primaries but the primaries in the data will cause artifacts. There are other artifacts that also come along with this method that have been noted in the literature.

The reality of today's methods for using multiples to predict missing "primaries" are aimed at structural improvement, at best, and are not claiming, seeking or delivering the amplitude and phase fidelity of the predicted primary. Those who go so far as to advocate using fewer sources and/or more widely separated cables because recorded multiples can produce "something like" a missing primary need to understand the deficits and costs including generating artifacts, less effectiveness with deeper primaries and the amplitude fidelity of the predicted primary. Whether the tradeoff makes sense ought to depend, in part, on the depth of the target, the type of play, and whether a structural interpretation or amplitude analysis is planned within a drilling program and decision.

By the way, this entire wave equation migration analysis (Claerbout

Imaging Condition III) is ultimately based on the idea from Green (1828) that to predict a wave (an experiment) inside a volume you need to know the properties of the medium in the volume.

There is an alternative view: The inverse scattering series methods communicates that all processing objectives can be achieved directly and without subsurface information. The inverse scattering series treat multiples as a form of coherent noise, and provide distinct subseries to remove free surface and internal multiples before the inverse scattering subseries for imaging and inversion achieve their goals using only primaries. If the inverse scattering series needed multiples to perform migration and inversion, it would not have provided subseries that remove those multiply reflected events. With a velocity model (wave equation migration) or without a velocity model (inverse scattering series imaging) only primaries are signal.

A key and essential point: conclusion

Hence, primaries are signal and multiples can be useful, at times, for predicting missing primaries. But it's primaries that are signal, that we use for structure and inversion.

Primaries are signal for all methods that seek to locate and identify targets.

The above three examples assumed you had an accurate **discontinuous** velocity and density model. Given an accurate discontinuous velocity and density model, and data with primaries and multiples, then we have convincingly demonstrated that only primaries contributed to the images at

every depth. If you predicted the source and receiver experiment at depth with a **smooth** velocity, it is possible to correctly locate (but not invert) each recorded primary event—but with a smooth velocity model every free surface and internal multiple will then produce a false image/artifact/event. If you removed the multiples first you can correctly locate structure from recorded primaries using a smooth velocity model.

Hence, we conclude that the inability, in practice, to provide an accurate discontinuous velocity model is why multiples need to be removed before imaging. That reality has been the case, is the case, and will remain true for the foreseeable future. Thats why multiples need to be removed before imaging. Multiples can at times be useful for creating missing primaries, **but once the primary is provided,** we don't want the multiples themselves involved when we seek to locate and identify structure.

Many things are useful for creating primaries: money, the seismic boat, the air-guns, the observer, the cable, computers, *etc.*, but we don't call all useful things signal.

Methods to provide a more complete set of primaries are to be supported and encouraged. Those methods include: (1) advances in and more complete acquisition, (2) interpolation and extrapolation methods, and (3) using multiples to predict missing primaries. However, a recorded primary is still the best and most accurate way to provide a primary, and the primary is the seismic signal.

A multiple can be useful, at times, for providing an unrecorded synthesized primary that is a subevent of the multiple. Given a data set consisting of: (1) the recorded primaries, (2) the synthesized primaries, (3) the

free surface multiples, and (4) internal multiples, the practical necessity of using a smooth continuous velocity for migration demands that all multiples be removed before migration. In exploration seismology, migration and migration-inversion are methods we employ to locate and identify structure. Claerbout Imaging Condition III is the most definitive and quantitative migration concept and procedure. This paper demonstrated that Claerbout Imaging Condition III clearly communicates that primaries are signal and multiples are noise.

Acknowledgements

M-OSRP sponsors are thanked for their encouragement and support. The author would like to thank Nizar Chemingui, Dan Whitmore and Alejandro Valenciano (PGS), Bob Stolt (ConocoPhillips, retired), Clement Kostov and Richard Coates (Schlumberger), and Jon Sheiman (Shell) for constructive and worthwhile discussions that benefited this paper. The author gratefully acknowledges PGS for showing how multiples can be used to predict unrecorded primaries, and Lundin Malaysia and PETRONAS for showrights. I would like to thank Yi Luo (Saudi Aramco) and David Monk and Bill Goodway (Apache Corp.) for stimulating and useful discussions that motivated and benefited this paper. The author would also thank Jinlong Yang, Jim Mayhan, Chao Ma, and Yanglei Zou for assistance in preparing this paper.

References

Amundsen, L., 1994, The propagator matrix related to the Kirchhoff-Helmholtz integral in inverse wavefield extrapolation: Geophysics, **59**, 1902–1910.

Berkhout, A. J., and D. J. Verschuur, 1994, Multiple technology: Part 2, Migration of multiple reflections: 64th Annual International Meeting, SEG, Expanded Abstracts, 1497–1500.

———, 1997, Estimation of multiple scattering by iterative inversion, Part I: Theoretical considerations: Geophysics, **62**, 1586–1595.

———, 2012, Full wavefield migration - utilization of multiples in seismic migration: Presented at the 74th EAGE Conference & Exhibition, Extended Abstracts.

Claerbout, J. F., 1971, Toward a unified theory of reflector mapping: Geophysics, **36**, 467–481.

Clayton, R. W., and R. H. Stolt, 1981, A Born-WKBJ inversion method for acoustic reflection data: Geophysics, **46**, 1559–1567.

Davydenko, M., and D. J. Verschuur, 2013a, Full wavefield migration, using internal multiples for undershooting: 73rd Annual International Meeting, SEG, Expanded Abstracts, 3741–3745.

———, 2013b, Full wavefield migration without dip limitation - using duplex waves in the imaging with multiples: Presented at the 75th EAGE Conference & Exhibition, Extended Abstracts.

Fleury, C., and R. Snieder, 2011, Reverse-time-migration of multiply scattered seismic waves: 81st Annual International Meeting, SEG, Expanded

Abstracts, 3382–3387.

———, 2012, Increasing illumination and sensitivity of reverse-time migration with internal multiples: Presented at the 74th EAGE Conference & Exhibition, Extended Abstracts.

Green, G., 1828, An essay on the application of mathematical analysis to the theories of electricity and magnetism: Privately published. (Available at http://babel.hathitrust.org/cgi/pt?id=hvd.yl131n;view=1up;seq=9).

Liu, F., and A. B. Weglein, 2013, The first *wave theory* RTM, examples with a layered medium, predicting the source and receiver at depth and then imaging, providing the correct location and reflection amplitude at every depth location, and where the data includes primaries and all internal multiples.: M-OSRP 2012-2013 Annual Report, 284–335.

———, 2014, The first wave equation migration RTM with data consisting of primaries and internal multiples: theory and 1D examples: Journal of Seismic Exploration, **23**, 357–366.

Loewenthal, D., L. Lu, R. Roberson, and J. W. C. Sherwood, 1985, The wave equation applied to migration: Geophysical Prospecting, **24**, 380–399.

Lu, S., and N. D. Whitmore, 2013, Effects of acquisition geometry to 3D separated wavefield imaging: Presented at the 75th EAGE Conference & Exhibition, Extended Abstracts.

Lu, S., N. D. Whitmore, H. LeGleut, and A. Long, 2013a, 3D high-resolution imaging using separated wavefields: Presented at the 75th EAGE Conference & Exhibition, Extended Abstracts.

Lu, S., N. D. Whitmore, and A. A. Valenciano, 2013b, Challenges and op-

portunities in 3D imaging of sea surface related multiples: 83rd Annual International Meeting, SEG, Expanded Abstracts, 4111–4115.

Lu, S., N. D. Whitmore, A. A. Valenciano, and N. Chemingui, 2011, Imaging of primaries and multiples with 3D SEAM synthetic: 81st Annual International Meeting, SEG, Expanded Abstracts, 3217–3221.

McMechan, G. A., 1983, Migration by extrapolation of time dependent boundary values: Geophysical Prospecting, **31**, 413–420.

Morse, P. M., and H. Feshbach, 1981, Methods of theoretical physics: Feshbach Publishing, LLC. (Original publication 1953 by The McGraw-Hill Companies, Inc.).

Ong, C., C. Lapilli, J. Perdomo, and R. Coates, 2013, Extended imaging and illumination in wave migrations: 83rd Annual International Meeting, SEG, Expanded Abstracts, 4116–4120.

Riley, D. C., and J. F. Claerbout, 1976, 2D multiple reflections: Geophysics, **41**, 592–620.

Schneider, W. A., 1978, Integral formulation for migration in two and three dimensions: Geophysics, **43**, 49–76.

Soni, A. K., X. Staal, and E. Verschuur, 2012, VSP imaging using all multiples: Full wavefield migration approach: 72nd Annual International Meeting, SEG, Expanded Abstracts, 1–6.

Stolt, R. H., 1978, Migration by Fourier transform: Geophysics, **43**, 23–48.

Stolt, R. H., and A. K. Benson, 1986, Seismic migration: theory and practice: Geophysical Press.

Stolt, R. H., and A. B. Weglein, 1985, Migration and inversion of seismic data: Geophysics, **50**, 2458–2472.

———, 2012, Seismic imaging and inversion: Application of linear inverse theory: Cambridge University Press.

Wang, Y., X. Chang, and H. Hu, 2013, Simultaneous reverse time migration of primaries and multiples without multiples prediction: Presented at the 75th EAGE Conference & Exhibition, Extended Abstracts.

———, 2014, Simultaneous reverse time migration of primaries and free-surface related multiples without multiple prediction: Geophysics, **79**, S1–S9.

Weglein, A. B., 2014a, Multiple attenuation: strategy that addresses current challenges: E&P Magazine, **87**, 132–135.

———, 2014b, Multiples: Signal or noise?: 84th Annual International Meeting, SEG, Expanded Abstracts, 4393–4399.

Weglein, A. B., and R. H. Stolt, 1999, Migration-inversion revisited (1999): The Leading Edge, **18**, 950–952, 975.

Weglein, A. B., R. H. Stolt, and J. D. Mayhan, 2011a, Reverse-time migration and Green's theorem: Part I — The evolution of concepts, and setting the stage for the new RTM method: Journal of Seismic Exploration, **20**, 73–90.

———, 2011b, Reverse time migration and Green's theorem: Part II — A new and consistent theory that progresses and corrects current RTM concepts and methods: Journal of Seismic Exploration, **20**, 135–159.

Whitmore, N. D., 1983, Iterative depth imaging by back time propagation: 53rd Annual International Meeting, SEG, Expanded Abstracts, 382–385.

Whitmore, N. D., A. Valenciano, S. Lu, and N. Chemingui, 2011a, Imaging of primaries and multiples with image space surface related multiple elim-

ination: Presented at the 73rd EAGE Conference & Exhibition, Extended Abstracts.

Whitmore, N. D., A. A. Valenciano, S. Lu, and N. Chemingui, 2011b, Deep water prestack imaging with primaries and multiples: Presented at the Twelfth International Congress of the Brazilian Geophysical Society, Sociedade Brasileira de Geofísica.

Whitmore, N. D., A. A. Valenciano, W. Sollner, and S. Lu, 2010, Imaging of primaries and multiples using a dual-sensor towed streamer: 80th Annual International Meeting, SEG, Expanded Abstracts, 3187–3192.

Figures

Figure 1: *The infinite hemispherical migration model. The measurement surface is denoted by MS.*

Figure 2: *A finite volume model.*

Figure 3: *1D upgoing plane wavefield.*

Figure 4: *Backpropagation model evolution.*

Figure 5: *Green's theorem predicts the wavefield at an arbitrary depth z between the shallower depth a and deeper depth b.*

Figure 6: *Imaging with primaries and internal multiples. A double Green's theorem is utilized with the data, and a Green's function that along with its normal derivative vanishes on the lower surface (and on the walls, in multi-D). That is what wave-equation migration means for waves that are two-way propagating in the medium.*

Figure 7:

Figure 8:

Figure 9:

Figure 10:

Figure 11:

Figure 12:

Figure 13:

Figure 14:

Figure 15:

Figure 16:

Figure 17:

Figure 18:

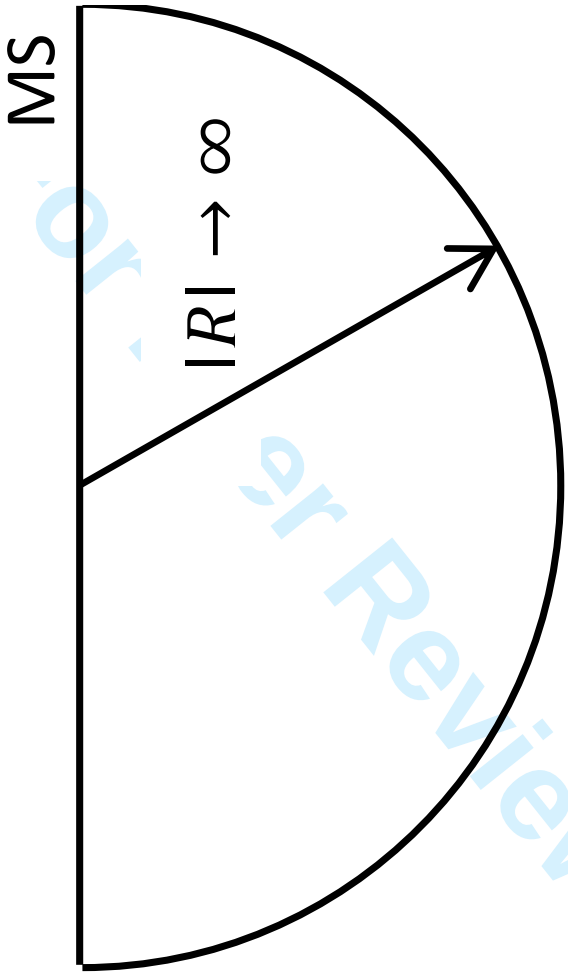

Figure 1: *The infinite hemispherical migration model. The measurement surface is denoted by MS.*

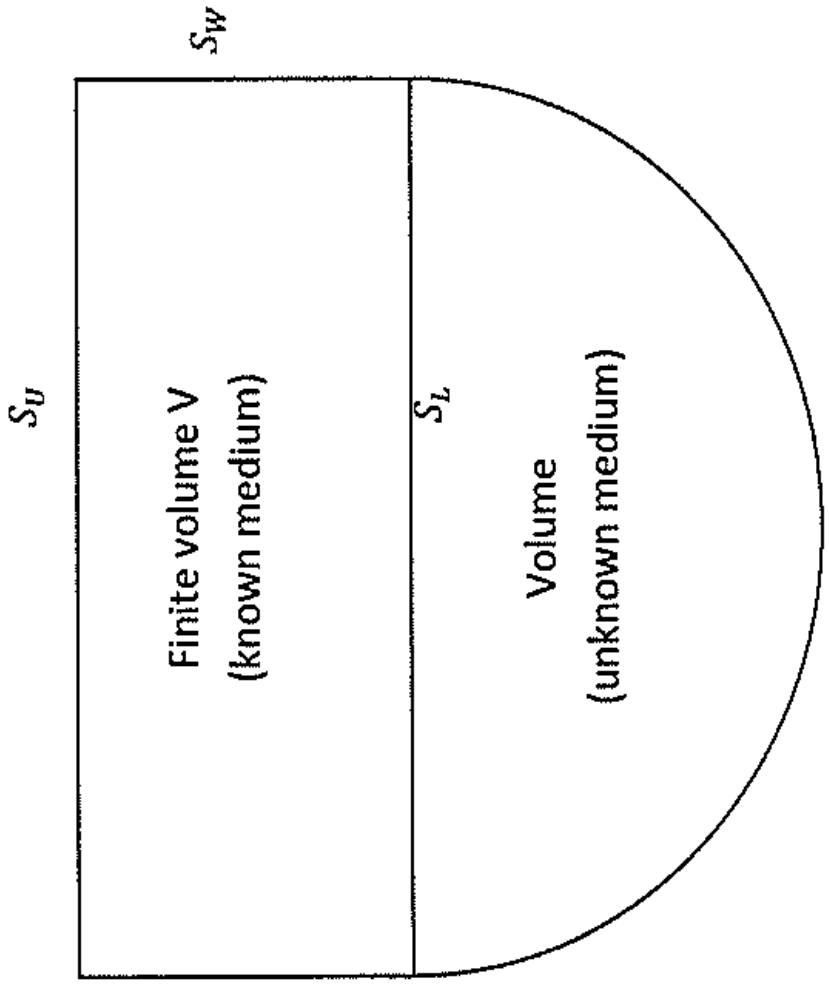

Figure 2: *A finite volume model.*

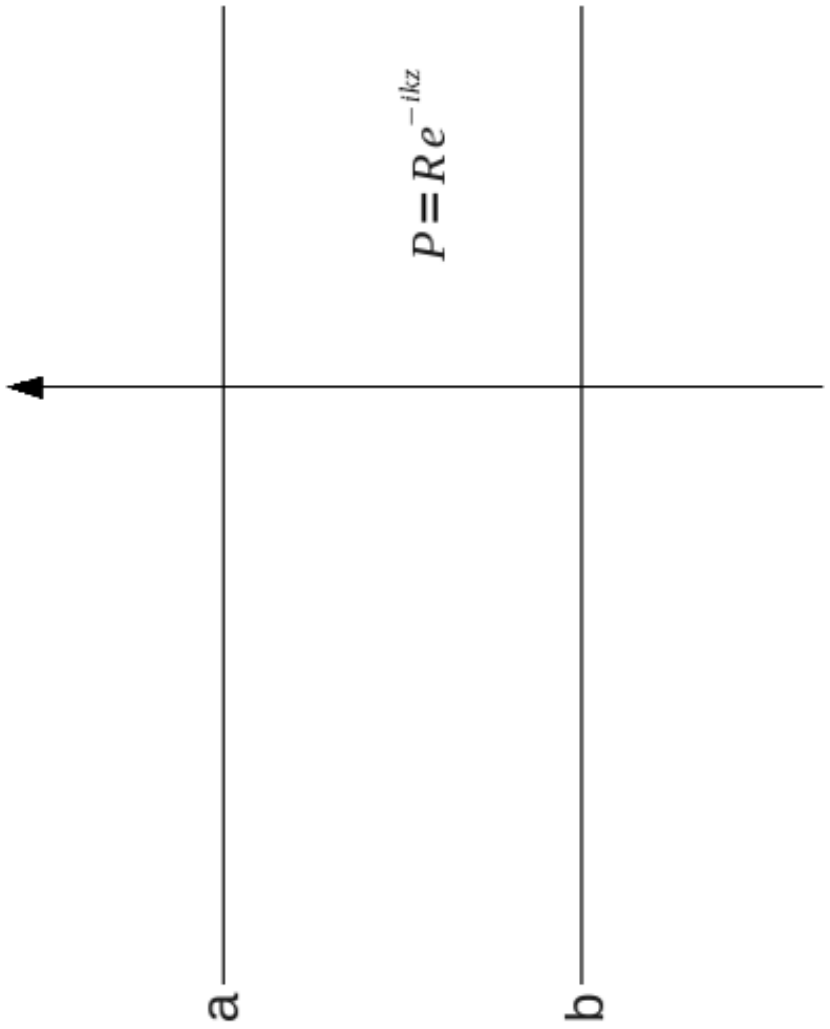

Figure 3: *1D upgoing plane wavefield.*

Figure 4: *Backpropagation model evolution.*

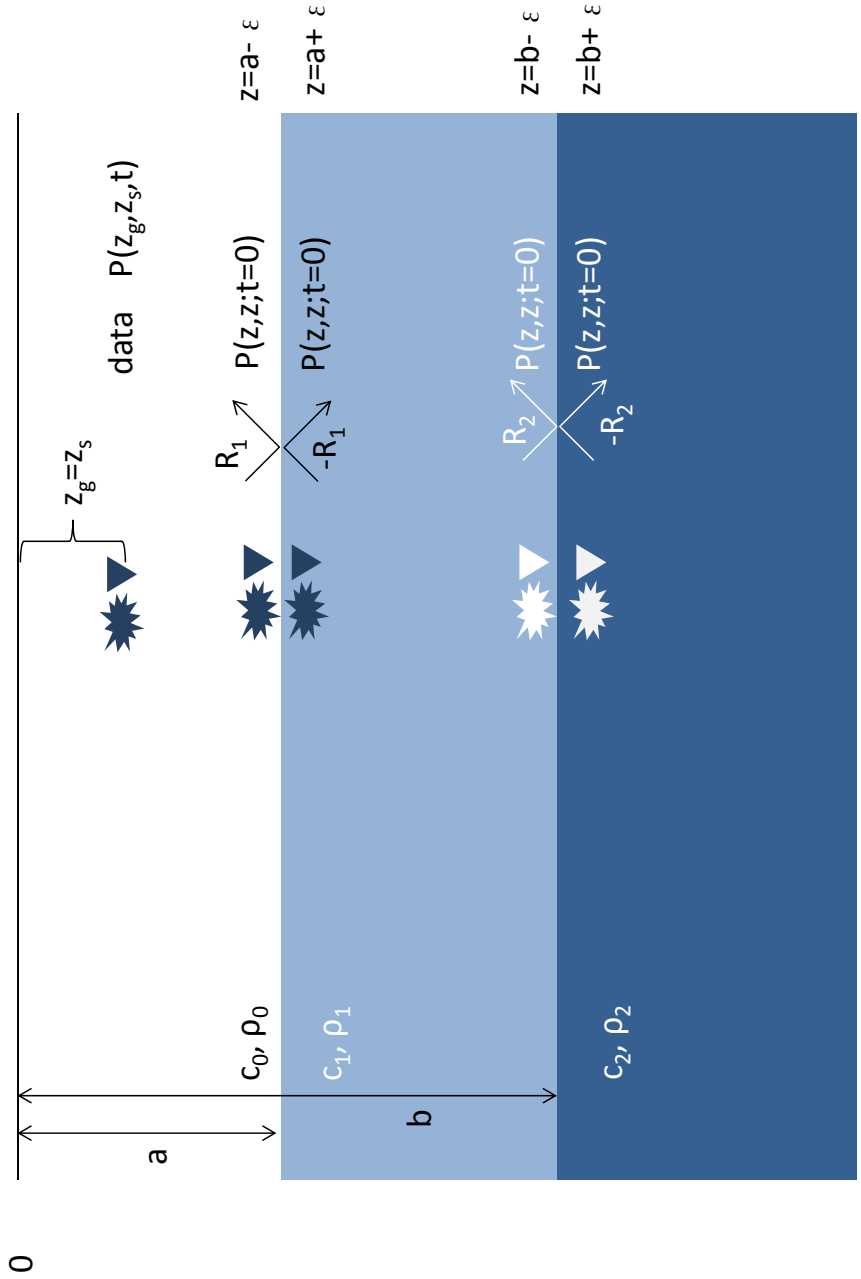

Figure 5: *Green's theorem predicts the wavefield at an arbitrary depth z between the shallower depth a and deeper depth b.*

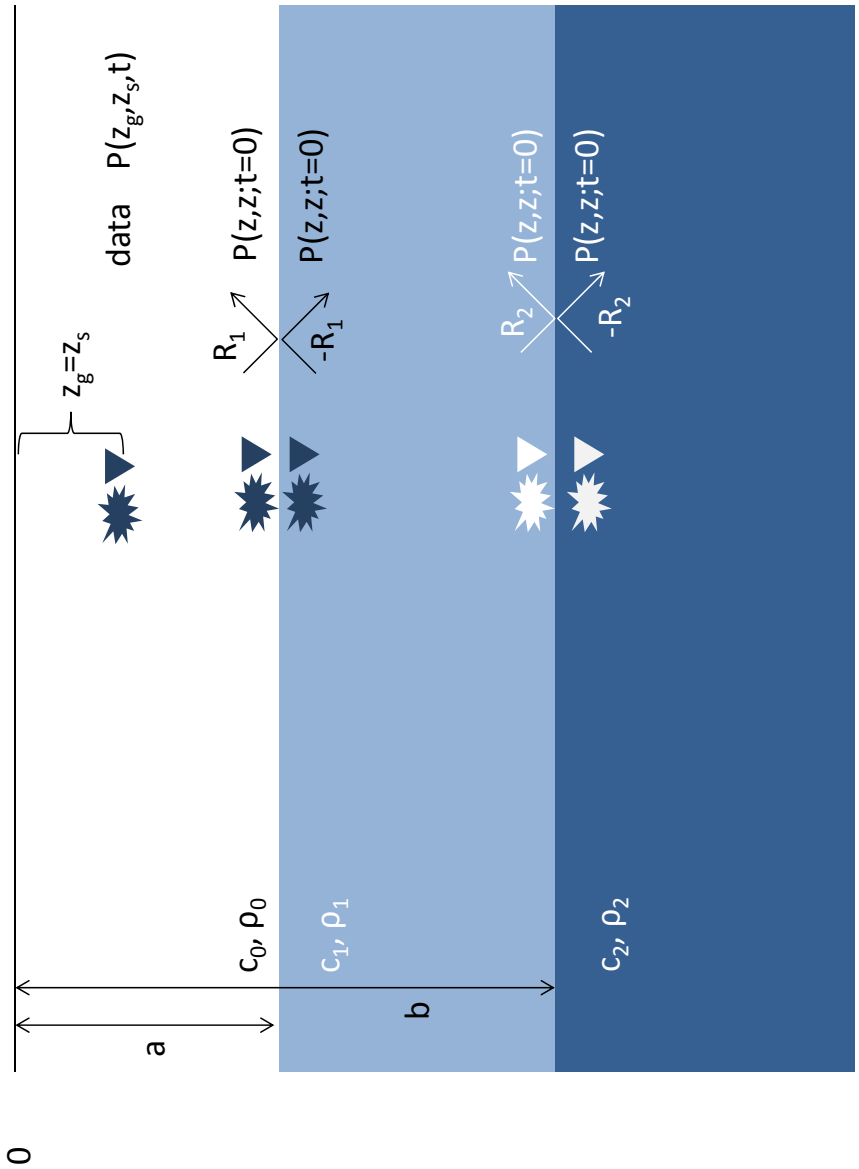

Figure 6: *Imaging with primaries and internal multiples. A double Green's theorem is utilized with the data, and a Green's function that along with its normal derivative vanishes on the lower surface (and on the walls, in multi-D). That is what wave-equation migration means for waves that are two-way propagating in the medium.*

Case 1: a primary from a single reflector (recorded data)
Reflector

Figure 7:

Case 1: a primary from a single reflector
Above the reflector (predicted experiment at depth)
Coincident source and receiver at depth for all times
Blue event: primary
Coincident source and receiver at depth for t = 0
R_1
Blue event: primary

Figure 8:

Case 1: a primary from a single reflector
Below the reflector (predicted experiment at depth)
Coincident source and receiver at depth for all times
Blue event: primary
Coincident source and receiver at depth for t = 0
$-R_1$
Blue event: primary

Figure 9:

Case 2: a primary and a free-surface multiple
(recorded data)
Free surface
Reflector
Red event: primary
Blue event: free-surface multiple

Figure 10:

Case 2: a primary and a free-surface multiple
Above the reflector (predicted experiment at depth)
Coincident source and receiver at depth for all times
Coincident source and receiver at depth for t = 0
R_1
Red event: primary
Blue event: free-surface multiple
Red event: primary

Figure 11:

Case 2: a primary and a free-surface multiple
Below the reflector (predicted experiment at depth)
Coincident source and receiver at depth for all times
Red event: primary (downward reflection at the reflector)
Blue event: primary (downward reflection at the free surface)
Coincident source and receiver at depth for t = 0
$-R_1$
Red event: primary (downward reflection at the reflector)

Figure 12:

Case 3: two primaries and an internal multiple
(recorded data)
Reflector 1
Reflector 2
Red event: primary from the first reflector
Black event: primary from the second reflector
Blue event: internal multiple

Figure 13:

Case 3: two primaries and an internal multiple
Above the first reflector (predicted experiment at depth)
Coincident source and receiver at depth for all times
Coincident source and receiver at depth for t = 0
R_1
Red event: primary from the first reflector
Black event: primary from the second reflector
Blue event: internal multiple
Red event: primary from the first reflector

Figure 14:

Case 3: two primaries and an internal multiple
Below the first reflector (predicted experiment at depth)
Coincident source and receiver at depth for all times
Coincident source and receiver at depth for t = 0
$-R_1$
Red event: primary from the first reflector
Black event: primary from the second reflector
Blue event: internal multiple
Red event: primary from the first reflector

Figure 15:

Case 3: two primaries and an internal multiple
Above the second reflector (predicted experiment at depth)
Coincident source and receiver at depth for all times
Coincident source and receiver at depth for t = 0
R_2
Red event: primary from the first reflector
Black event: primary from the second reflector
Blue event: internal multiple
Black event: primary from the second reflector

Figure 16:

Case 3: two primaries and an internal multiple
Below the second reflector (predicted experiment at depth)
Coincident source and receiver at depth for all times
Coincident source and receiver at depth for t = 0
$-R_2$
Blue event: primary from the first reflector
Black event: primary from the second reflector
Black event: primary from the second reflector

Figure 17:

Figure 18: